Nitrogen doped n-type amorphous carbon films obtained by pulsed laser deposition with a natural camphor source target for solar cell applications

2005 J. Phys.: Condens. Matter 17 1929

(http://iopscience.iop.org/0953-8984/17/12/016)

INSTITUTE OF PHYSICS PUBLISHING JOURNAL OF PHYSICS: CONDENSED MATTER

J. Phys.: Condens. Matter **17** (2005) 1929–1946 doi:10.1088/0953-8984/17/12/016

Nitrogen doped n-type amorphous carbon films obtained by pulsed laser deposition with a natural camphor source target for solar cell applications

M Rusop[1], S M Mominuzzaman[2], T Soga[1], T Jimbo[1] and M Umeno[3]

[1] Department of Environmental Technology and Urban Planning, Nagoya Institute of Technology, Nagoya 466-8555, Showa-ku, Gokiso-cho, Japan
[2] Department of Electrical and Electronic Engineering, Bangladesh University of Engineering and Technology, Dhaka 1000, Bangladesh
[3] Department of Electronic Engineering, Chubu University, Kasugai 487-8501, Matsumoto-cho 1200, Japan

E-mail: hambalah@gmail.com (M Rusop)

Received 2 September 2004, in final form 7 February 2005
Published 11 March 2005
Online at stacks.iop.org/JPhysCM/17/1929

Abstract

Nitrogen doped n-type amorphous carbon (n-C:N) films are deposited by a pulsed laser deposition technique at room temperature using a camphoric carbon target with different nitrogen partial pressures (NP) in the range from 0.1 to 800 mTorr. The room temperature conductivity (σ_{RT}) is found to increase with N incorporation perhaps due to increasing density of trihedral (sp^2) hybridization of electronic states, for NP increasing from 1 to 30 mTorr, as shown by x-ray photoelectron spectroscopy (XPS), Fourier transform infrared spectroscopy (FTIR), and optical data relevant to band tails. Study of the activation energy reveals that the Fermi level of the n-C:N film moves from the valence band to near the conduction band edge through the mid-gap. The current–voltage photovoltaic characteristics of n-C:N/p-Si cells under 1 sun air-mass 1.5 (AM 1.5) illumination conditions (100 mW cm^{-2}, 25 °C) are improved up to 30 mTorr and deteriorate subsequently. The maximum open circuit voltage (V_{oc}) and short circuit current density (J_{sc}) for the cells are observed to be approximately 292 mV and 9.02 mA cm^{-2}, respectively. The highest energy conversion efficiency (η) and fill factor (FF) were found to be approximately 1.47% and 56%, respectively.

(Some figures in this article are in colour only in the electronic version)

1. Introduction

Amorphous carbon (a-C) shows a semiconducting nature, which promotes its application in the field of semiconductor technology, such as in fabrication of photovoltaic solar cells [1].

However, undoped a-C is weakly p-type [1] in nature, and the complex structure and presence of a high density of defects restrict its ability to dope efficiently and are the main barriers to its application in various electronic devices; therefore, when we attempt to utilize such carbon as an alternative material in optoelectronic devices, control of the conduction type through doping of the carbon film is indispensable. The doping mechanism of amorphous semiconductors has always been an interesting issue. Observations from the literature show that the semiconducting carbon films can be either intrinsic or doped during or after the growth to make them extrinsic semiconductors. Effective doping can modify electronic properties, especially gap states, conductivity, etc, in semiconductor materials. Many attempts have been made to dope carbon films using various elements.

It has been reported that phosphorus (P) is the most widely used n-type impurity in silicon [2] and is a possible alternative to N in carbon [2]. However, since N has a smaller radius compared to P, close to that of carbon, the former would be preferred. Further, N being gas phase has the advantage of better control of dopant concentration over P in physical deposition systems. Veerasamy *et al* reported n-type doping of highly tetrahedral carbon (ta-C) using solid P [1] and n-type doping in a-C using N gas [3–5], while other authors [6, 7] reported N as the common dopant in carbon films with few exceptions. The ability to dope [8] using N gas and P has shown a new direction for the application of carbonaceous material in electronic devices. However, P and N doping of carbon in order to convert undoped p-type conductivity carbon to n-type [9], in the relatively small gap of DLC film with an optical gap close to that of single-crystal silicon (1.1 eV), which has scope for optoelectronic device applications using the PLD technique, has not been reported so far.

In this paper, the doping modifications of the temperature dependence and photovoltaic properties that occur in nitrogen doped n-type amorphous carbon (n-C:N) films when they are deposited at different NP have been investigated and discussed. The objective of this study is to dope slightly p-type a-C to electrically semiconducting n-C:N for possible application as semiconductors and optoelectronic devices.

2. Experimental details

The n-C:N films were deposited on single-crystal silicon (100) and fused quartz substrates by xenon chloride (XeCl) excimer pulsed laser deposition (figure 1, PLD, NISSIN 10X, $\lambda = 308$ nm, $\tau = 20$ ns), which is focused on the target by an ultraviolet grade plano-convex lens at an incidence angle of 45° to the target normal, using a camphoric carbon (CC) target [9] at room temperature with different nitrogen partial pressures (NP). In this research, camphor ($C_{10}H_{16}O$) has been used as a new starting precursor and as a source of material for the deposition of suitable carbonaceous films for future application in optoelectronic devices. The CC soots are obtained from burning camphor, a natural source, abundantly available in nature, economically cheap, non-toxic, and harmless, which is the main objective of this research along with the low cost productive materials. The CC soots might be a new precursor material because it also has hydrogen (H) abundantly in its structure (figure 2).

A schematic representation of the experimental set-up constructed for the generation of carbon soot by burning camphor is shown in figure 3. Camphor is burned in a 1 m long and 11 cm diameter quartz cylinder tube. A rotary pump is used to suck the air from the burning system and maintain continuous circulation of air to facilitate camphor burning. A filter is used to filter the soot and clean the mixed air. Cold water flow is maintained to keep the wall of the cylinder tube cold and not heated up. The CC soot deposited along the inside walls of the cylinder tube and the filter was collected, dried in the oven for an hour, and pressed into pellets with a hydraulic presser of load 4.5 tons for approximately 2 min in order to allow us to

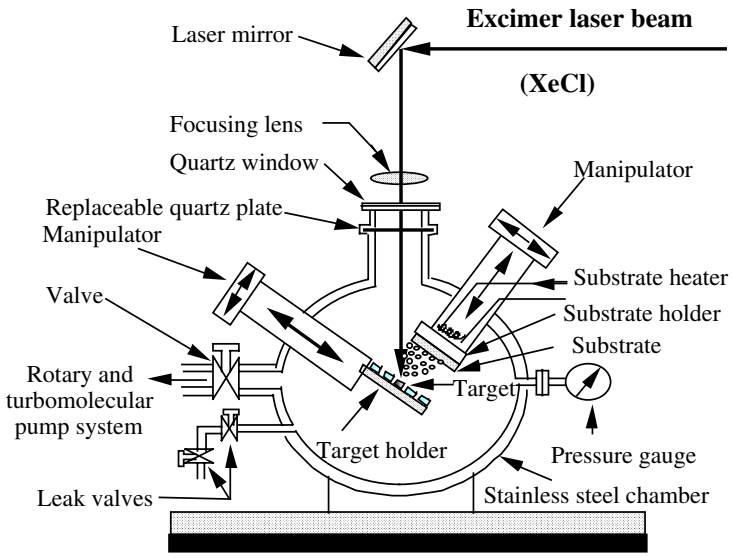

Figure 1. Schematic representation of the pulsed laser deposition chamber system.

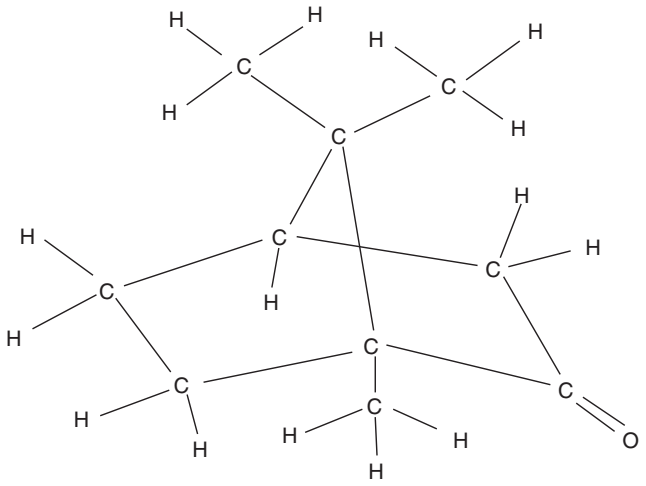

Figure 2. Chemical structure of the camphor molecule ($C_{10}H_{16}O$).

use them as a targets. These pellets were used as targets in the PLD process for the deposition of carbonaceous films.

NP in the range from 0.1 to 800 mTorr using a CC target in the N-doping modification of a-C films has been investigated. The ambient gas was introduced into the PLD chamber via a leak valve. The target for each deposition method was ablated with 175 mJ/pulse average laser pulse energy with an average laser fluence of 3.4 J cm^{-2}, laser shots of 900 shots, and laser repetition rates of 2 Hz. The substrate is mounted on a metal substrate stage holder parallel to the target, in which the target to substrate distance was set at a distance of 45 mm. The substrate temperature (ST) was fixed at room temperature 25 °C by the substrate heater automatic controller.

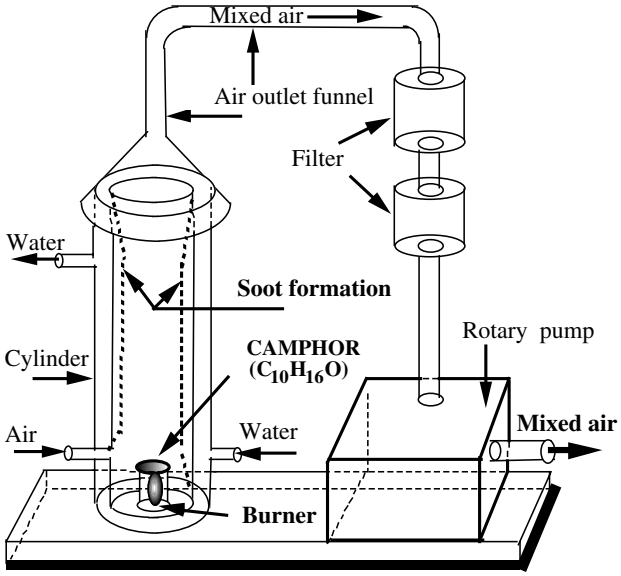

Figure 3. Schematic representation of the camphor burning system.

Before deposition of each experimental sample, the silicon (Si) and glass substrates were cleaned with acetone and methanol in a hot water bath at 55 °C for 5 min. After cleaning, they were etched with HF:H_2O (1:10) in order to remove the resistive native oxide formed over the surface, and quickly transferred into the PLD chamber. In order to ensure a uniform ablation rate, for each experiment the target is rotated every 50 shots during the deposition. The deposition system is stainless steel with a high vacuum chamber (under 2×10^{-6} Torr) that is initially evacuated for 4 h using a turbomolecular pump and, after that, N gas ambient was allowed until the chamber pressure was constant at the setting value of NP. For comparison, the undoped a-C film was also deposited using a pure CC target, hereafter also referred to as sample A. All the films and photovoltaic cells were analysed by using standard experimental characterization techniques [9].

3. Results and discussion

The thicknesses of the deposited sample A and n-C:N films are measured, for each of the films deposited on the Si substrates, by an Alpha-Step 500 profiler. The maximum average deposition rate (nm/shot; figure 4 (right axis)) was calculated as the quotient of the measured maximum thickness (nm) and the number of pulses (shots) applied. The thickness and deposition rate for sample A deposited on Si are found to be approximately 200 nm and 0.22 nm/shot. The deposition rate of sample A (deposited using CC target) is about 10 times higher than that of the a-C film deposited on Si substrate by PLD using a graphite target [10]. The low and different deposition rate on Si substrate compared with the CC film (sample A) case may be reflected by the low energy of the species ablated from the graphite target. Thus, comparing these results with the earlier observations for glassy carbon and graphite targets [10], the kinetic energy of the CC species would be considered higher than that for graphite. The higher kinetic energy could then help with the formation of better quality a-C films.

As shown in figure 4 (right axis), the deposition rate for n-C:N films deposited on Si substrates is found to decreased about linearly, proportionally to the increase of NP, in the

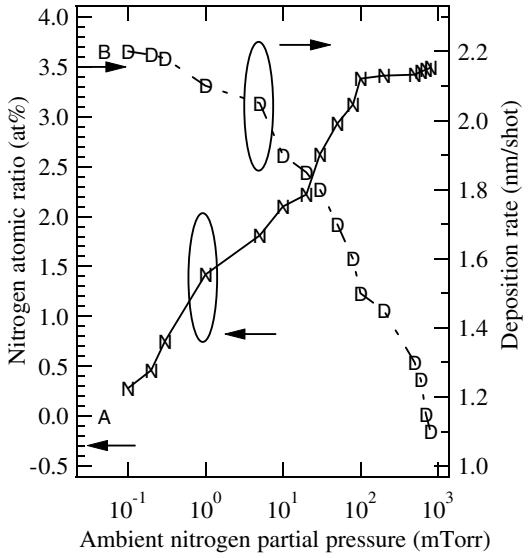

Figure 4. Nitrogen atomic percentage (at.%) (left axis) and deposition rate (nm s^{-1}) (right axis) of sample A, and n-C:N films deposited at various ambient nitrogen partial pressures. (Left axis: A for sample A, and N for a-C:N films. Right axis: B for sample A, and D for a-C:N films.)

chamber up to 0.11 nm/shot at 800 mTorr. The decrease of the deposition rate may be due to increase in atomic collisions before deposition with increase of NP in the chamber. It also could be related to the ablation mechanism of the XeCl excimer laser that is used in this system (PLD) with the wavelength of 308 nm, as described in the literature [11].

The surface morphologies of the films were examined to clarify whether there is atomic structural modification in the a-C films such as graphitization during N addition [9, 12]. SEM and AFM (figure 5) show that the surface morphology of n-C:N film deposited at 0.1 mTorr was smooth (R_a: 4.87 nm, rms: 6.21 nm) compared with that of sample A (R_a: 6.97 nm, rms: 8.89 nm). The particle size, surface roughness (R_a), and average roughness estimated over 1 μm $\times$ 1 μm area (root mean square, rms) decrease initially at 0.1 mTorr and, obviously unchanged, do not differ markedly with the NP addition up to 1 mTorr (R_a: 5.01 nm, rms: 6.45 nm), suggesting there is no crystallization and atomic structural change due to N addition up to 1 mTorr. Above 1 mTorr the particle size has increased while the density of the particles and the surface roughness have increased; this implies that some small particles have merged into a large particle due to the enhanced surface migration of the deposited CC species, suggesting there is a crystallization due to N addition higher than 1 mTorr. However, above 30 mTorr, the n-C:N films become smoother with increase of NP, indicating that there is a atomic structural changing.

Compositional chemical analyses of the deposited films were performed by Auger electron spectroscopy (AES). The AES spectrum of each film was taken without etching at 10^{-7} Pa chamber pressure. Figure 6 illustrates that C and N were detected in the AES spectra at about 284 and 398 eV, respectively, showing that the sample A and n-C:N films were mainly composed of C, and C and N, respectively. The existence of a small oxygen signal was detected in all the spectra of the sample A and n-C:N films at about 532 eV, as a result of contamination and air exposure during sample transport.

Although there are still some controversies about the assignments of the individual components of the C 1s and N 1s core level spectra [13–15], the x-ray photoelectron

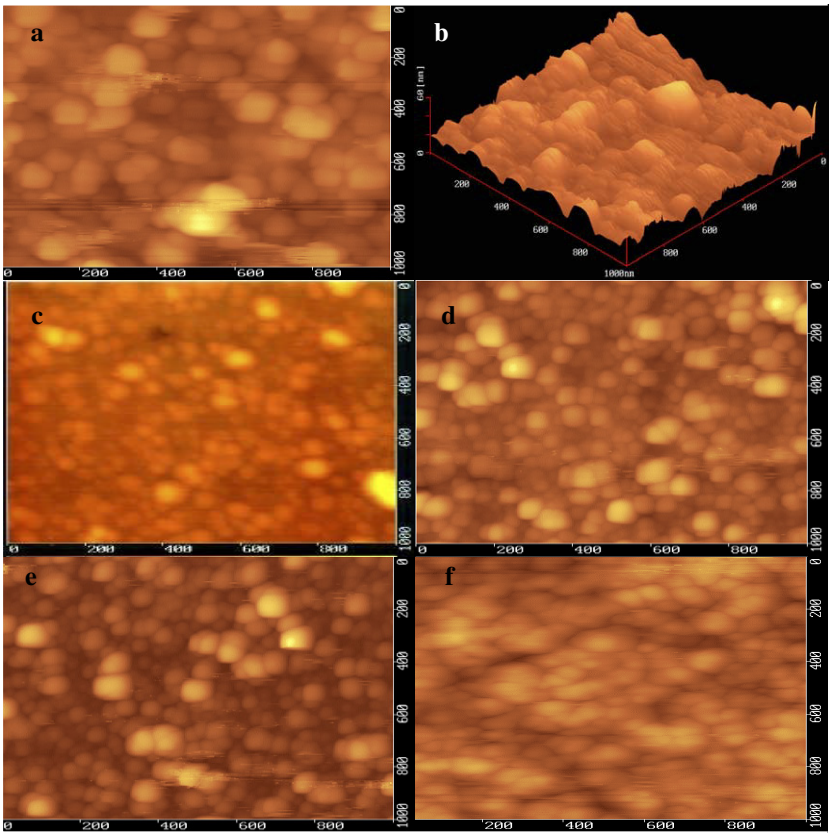

Figure 5. AFM images, on Si substrates, for (a) sample A (2D) ($R_a = 6.97$ nm, rms = 8.89 nm), (b) sample A (3D), and n-C:N films deposited in ambient: (c) 0.1 mTorr ($R_a = 4.87$ nm, rms = 6.21 nm), (d) 0.3 mTorr ($R_a = 4.92$ nm, rms = 6.32 nm), (e) 1 mTorr ($R_a = 5.01$ nm, rms = 6.45 nm), and (f) 20 mTorr ($R_a = 7.85$ nm, rms = 9.87 nm) nitrogen partial pressures. (Scan area: 1 μm × 1 μm.)

spectroscopy (XPS) analysis is one of the most commonly used techniques in the literature for characterizing the formation; bond types and useful information on the chemical environment around O, C, and N for CN phases can be obtained. XPS was performed using an SSX-100 XPS system from Surface Science Instruments using Al Kα ($h\nu = 1486.6$ eV) radiation as an x-ray source, under high vacuum conditions of about 10^{-10} Torr. The chemical bonding states in the films were analysed after 0.5 keV Ar^+ ion etching of the film surface for 3 min.

The chemical composition of the deposited films can be obtained according to the oxygen to C (O/C) and the N to C atomic ratios (N/C). The N/C and O/C contents in the films were evaluated using $N/C = (A_N/1.68)/(A_C/1.00)$ and $O/C = (A_O/2.49)/(A_C/1.00)$ where A_N, A_O, and A_C are the areas under the N 1s, O 1s, and C 1s core level spectra and the constants 1.68, 2.49, and 1.00 are the atomic sensitivity factors of N, O, and C, respectively.

XPS shows that the C 1s peak position is increased to 284.9 eV (sample A: 284.8 eV; graphite: 284.25 eV; and diamond: 285.8 eV) at 0.1 mTorr, which may be due to the formation of a C–N bond which causes the tetrahedral (sp^3) bond increase [9]. The C 1s and N 1s peaks are almost unchanged up to 1 mTorr. With further increase of NP, the C 1s peak shifts toward lower binding energy and approaches the binding energy of graphite, 284.35 eV at 30 mTorr (figures 7

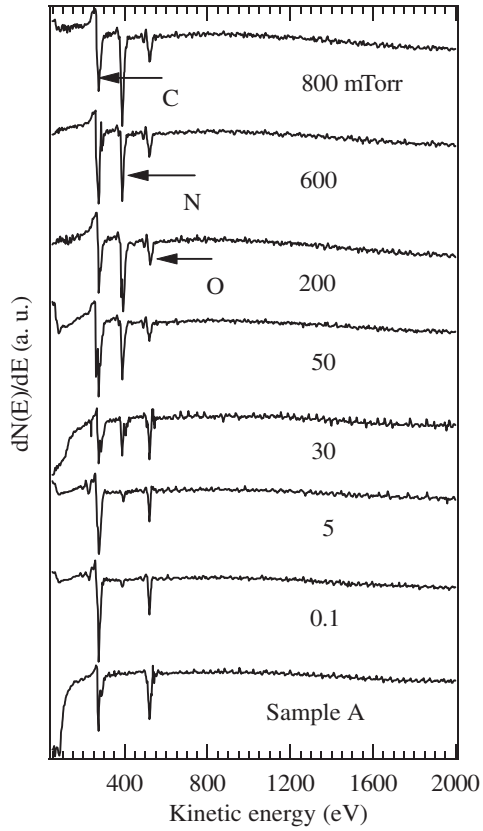

Figure 6. AES spectra of sample A, and a-C:N films deposited in various ambient nitrogen partial pressures.

and 8). This indicates that the bonding state of the films changes from low diamond-like sp^3 bonding to graphite-like trihedral sp^2 bonding. Above 30 mTorr, the C 1s peak shifts toward higher binding energy and reaches 284.6 eV at 800 mTorr. This indicates that the bonding state of the films changes from graphite-like sp^2 bonding to diamond-like sp^3 bonding. The presence of oxygen at approximately 0.25 at.% for each sample is probably related to the incorporation of oxygen due to prolonged exposure of the samples to the experimental atmosphere before XPS measurements and accidental incorporation during deposition [9]. As shown in figure 4 (left axis), the atomic percentage (at.%) of N/C (N content) in the n-C:N films increased rapidly initially up to about 2.93 at.% at 50 mTorr. With further increase of NP, the N content increases to about 3.41 at.% at 200 mTorr, and saturates thereupon, reaching about 3.49 at.% at 800 mTorr.

The bonding states of carbon (C), nitrogen (N), and hydrogen (H) atoms can be characterized by Fourier transform infrared spectroscopy (FTIR) measurements. Figure 9 shows FTIR transmittance spectra measured in the wavenumber range 600–2500 cm^{-1} for sample A and n-C:N films with various NP values. Band 1 at around 700 cm^{-1} is due to the out-of-plane bending mode for the graphite-like domain [8]. Broad absorption band 2 at 1000–1700 cm^{-1} indicates that the film structure is predominantly amorphous with sp^2 C vibration modes, and is related to Raman active D and G modes [9]. Other authors reported that the contributions around 1350 and 1550 cm^{-1} were initiated from disordered (D band)

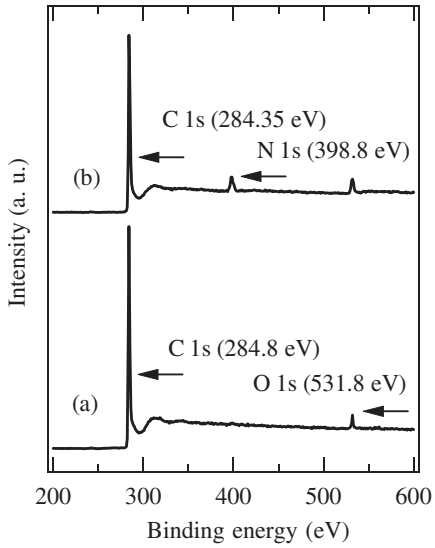

Figure 7. Core level x-ray photoelectron spectra of carbon (C 1s), nitrogen (N 1s), and oxygen (O 1s) for (a) sample A, and (b) n-C:N film deposited at 30 mTorr.

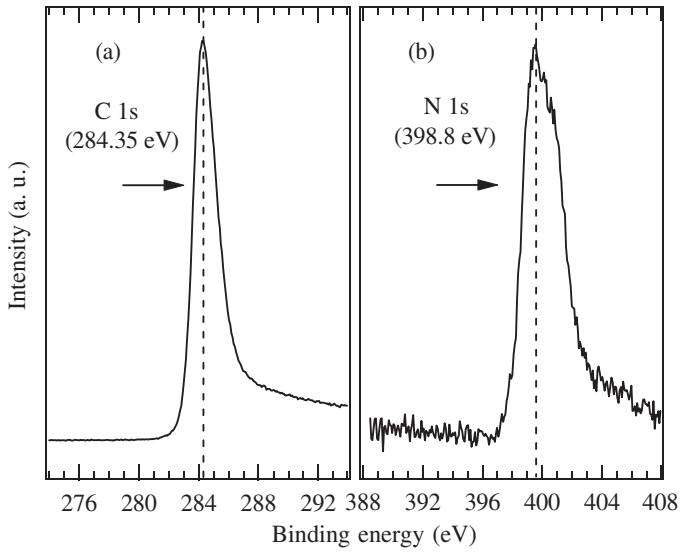

Figure 8. Core level x-ray photoelectron spectra of (a) carbon (C 1s) and (b) nitrogen (N 1s) for n-C:N film deposited at 30 mTorr.

and graphite-like (G band) CN bonds [6], respectively. Band 3 at 1100–1400 cm^{-1}, band 4 at 1500–1700 cm^{-1}, and band 5 at around 2200 cm^{-1} are due to C–N, C=C, and/or C=N and C≡N stretching vibration modes, respectively [10]. Other authors also reported the contribution at around 1212–1265 cm^{-1} as due to the symmetric tetrahedral CN bond [7].

As shown in figure 9, at 0.1 mTorr a single broad band centred at around 1365 cm^{-1}, almost unchanged up to 1 mTorr, was rapidly shifted later at 10 mTorr into a single broad band centred at around 1550 cm^{-1}. The FTIR absorption, almost unchanged with increase

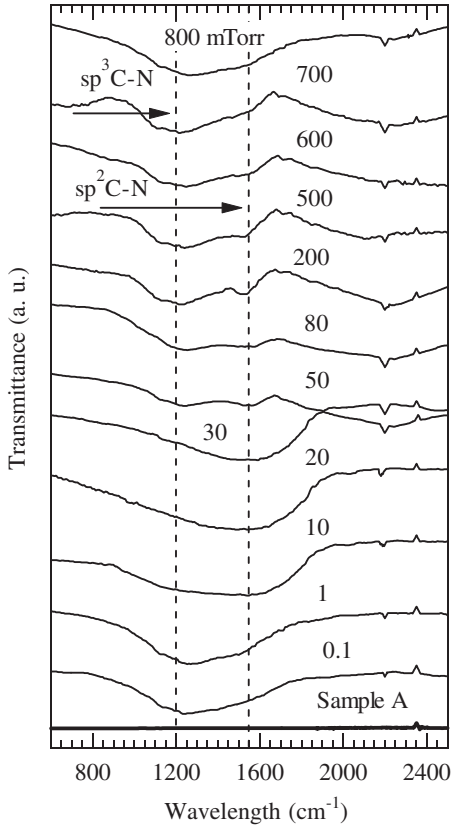

Figure 9. FTIR spectra of sample A, and n-C:N films with their corresponding ambient nitrogen partial pressures.

in NP up to 30 mTorr, was gradually resolved into two smaller bands located at 1550 and 1200 cm^{-1}. With increasing NP, these two bands became more prominent but transformed later, at 600 mTorr, into a single broad band centred at around 1200 cm^{-1}, and were almost unchanged with increase in NP thereafter. Above 30 mTorr, the G band seems to be suppressed gradually; this occurs together with the enhancement of the sp^3 C–N bonds. This indicates no modification of the binding geometry at low NP up to 1 mTorr and a modification of the binding geometry with the transformation of the sp^3 C–N bonds into sp^2 C–N binding state as NP is increased up to 10 mTorr, and almost stable conditions for the addition of NP up to 30 mTorr, whereas there is a modification of the binding geometry with the transformation of the sp^2 C–N bonds into the sp^3 C–N binding state as NP is increased up to 600 mTorr, and almost stable conditions for the addition of NP up to 800 mTorr.

This indicates the components of the C–N, C=N, C=C and C≡N bonds presents in our films in which it might contribute to the electrical properties of the n-C:N films. The electrical properties of the n-C:N films will be discussed in detail in the next chapter. This result further supports the presence of an N atomic ratio in the films, as we have discussed in the previous section using the XPS analyses. The broad band between 1000 and 1700 cm^{-1} and the band centred at 2200 cm^{-1} do not appear in sample A. The absorption peak at around 2350 cm^{-1}, which is observed for sample A and n-C:N films, can be attributed to the CO_2 stretching mode arising from oxygen contamination at the film surface [11].

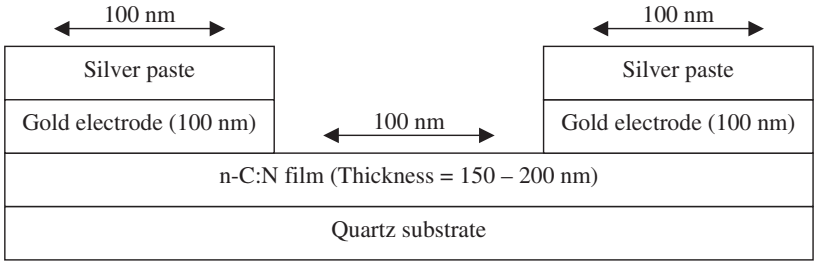

Figure 10. The schematic gap cell configuration for temperature dependent conductivity measurements of n-C:N films deposited under various ambient nitrogen partial pressures.

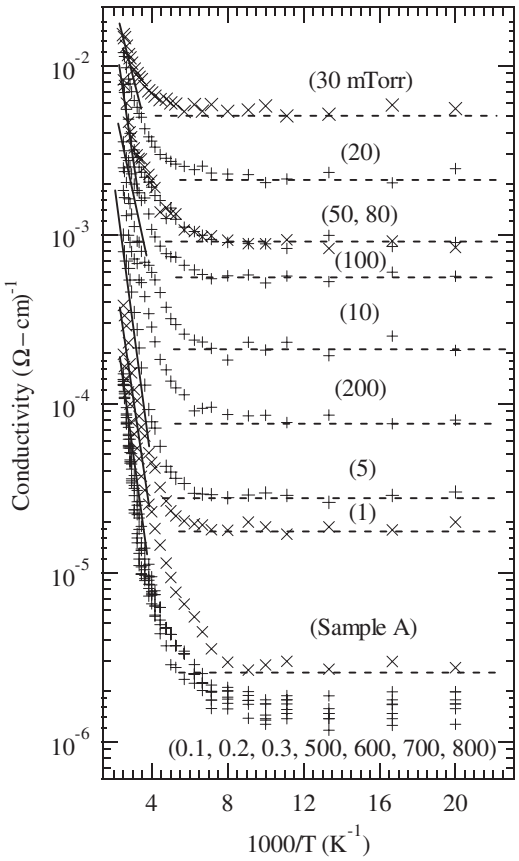

Figure 11. Temperature dependent conductivity of sample A, and n-C:N films deposited under various ambient nitrogen partial pressures.

The Tektronix VX1410 Intelli Frame from Sony was used for current–voltage (I–V) measurement and the Cryomini Compressor from Iwatani Plantech was used to maintain the temperature of the chamber (hereafter, this is also referred to as the two-probe method). The electron-beam-evaporated gold electrodes (thickness = 100 nm) were used in a gap–cell configuration and silver paste was used as a point contact on gold electrodes for conductivity measurements (figure 10). Using the results of the measurements, the electrical conductivity (σ) is plotted against inverse temperature (T) on a logarithmic scale. As shown in figure 11, σ

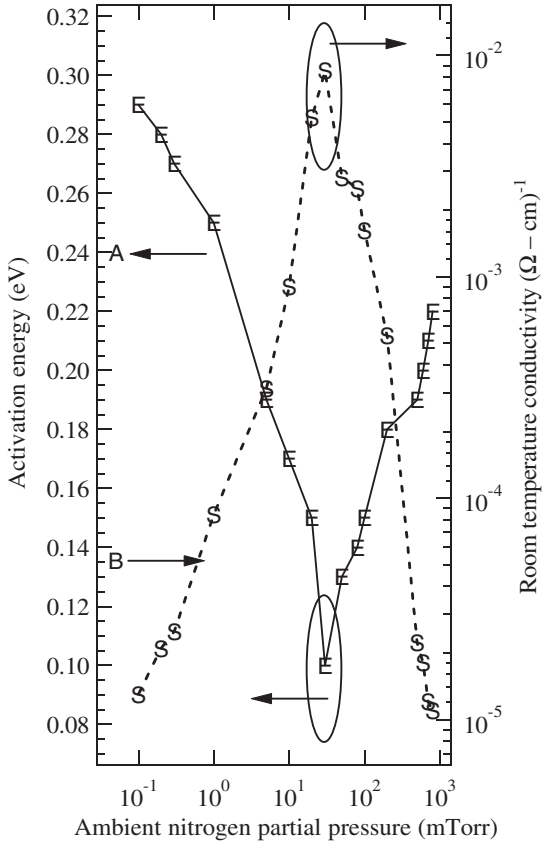

Figure 12. Activation energy (E_a) and room temperature conductivity (σ_{RT}) for sample A, and n-C:N films deposited in various ambient nitrogen partial pressures. (Left axis: E_a for sample A (A) and n-C:N films (E). Right axis: σ_{RT} for sample A (B) and n-C:N films measured by the two-probe method (S).)

for the films was measured as a function of T between 50 and 400 K. The T dependence of σ shows two regions, the 50–300 K range (variable range hopping) and the above 300 K range (simple activation region), which indicate domination of the hopping conductivity of the films.

The conductivity plotted in figure 11 does not follow the simple activated form of $\sigma(T) = \sigma_{01}\exp(-E_a/kT)$, where σ_{01} is the conductivity prefactor, T is the absolute temperature, k is Boltzmann's constant, and E_a is the activation energy with respect to the Fermi level, E_F [12]. Since a linear region is not observed for any particular range of temperature, activation energies E_a are determined from the slope of the straight parts of the logarithmic conductivity curves plotted as a function of inverse temperature from the highest temperature side [12] of the two temperature regions (400 K $\geqslant T >$ 300 K and 300 K $\geqslant T \geqslant$ 50 K).

Therefore, the activation energy (E_a) is determined from the slope of $\ln\sigma$ versus $1/T$ for the above room temperature (RT) region [9, 12]. The variations of E_a and the RT conductivity (σ_{RT}) as functions of NP are shown in figure 12 (left axis) and figure 12 (right axis), respectively. At 0.1 mTorr, E_a is increased to 0.29 eV (sample A: 0.24 eV), whereas σ_{RT} is decreased to 1.3×10^{-5} $(\Omega\ \mathrm{cm})^{-1}$ (sample A: 5.2×10^{-5} $(\Omega\ \mathrm{cm})^{-1}$). With further increase of NP up to 30 mTorr, E_a decreases, whereas σ_{RT} increases gradually and sharply thereafter. Above 30 mTorr, E_a and σ_{RT} increase with NP.

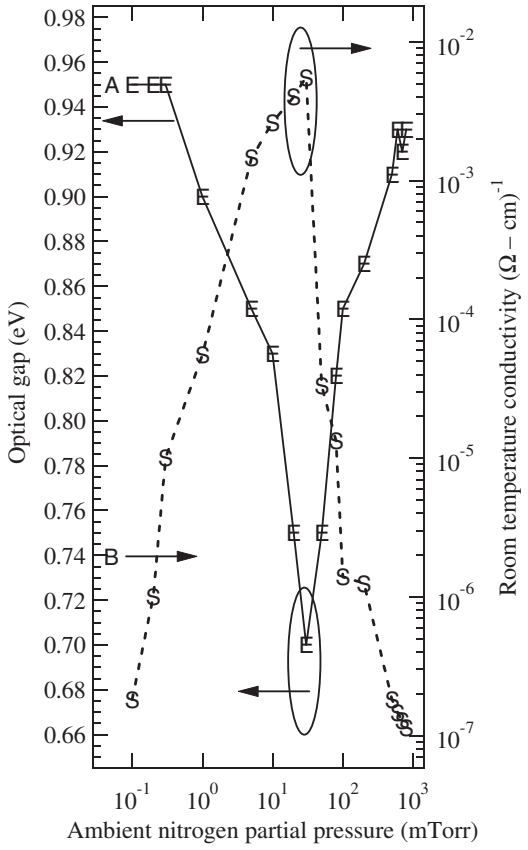

Figure 13. Optical gap (E_g) for sample A and n-C:N films deposited in various ambient nitrogen partial pressures. Left axis: E_g for sample A (A) and n-C:N films (E). Right axis: σ_{RT} for sample A (B) and n-C:N films measured by the four-point probe method (S).

For comparison, σ_{RT} has also been measured by using the four-point probe resistance measurement (hereafter, also referred to as the four-probe method). σ_{RT} measured by the four-probe method (figure 13 (right axis)) also shows almost the same conductivity characteristics as σ_{RT} measured by the two-probe method (figure 12 (left axis)), with maximum conductivity for the n-C:N films deposited at 30 mTorr, decreasing with reducing and increasing NP.

The optical properties of the films are investigated by means of UV–visible spectroscopy measurements in the range of 200–2500 nm. The Tauc relationship [16] was used to evaluate the optical band gap (E_g). The Tauc optical gap was plotted as a function of NP, as shown in figure 13 (left axis). As shown in figure 13 (left axis), the E_g for n-C:N films is almost unchanged up to 1 mTorr (sample A: 0.95 eV), but decreases thereafter to 0.83 eV at 10 mTorr, after which it decreases rapidly to 0.7 eV at 30 mTorr. With increasing NP, it increases to 0.91 eV at 500 mTorr and is almost constant thereafter to 0.93 eV at 800 mTorr, as can be estimated from the Tauc plot.

The variation of the optical band edge is attributed to the removal or creation of band tail states [17, 18], and the material is assumed to have fewer band tail states when the edge has an increase in slope. Figures 14 and 15 illustrate the dependence of the optical absorption edge on the NP, as a function of photon energy and wavelength, respectively. The slope increases from

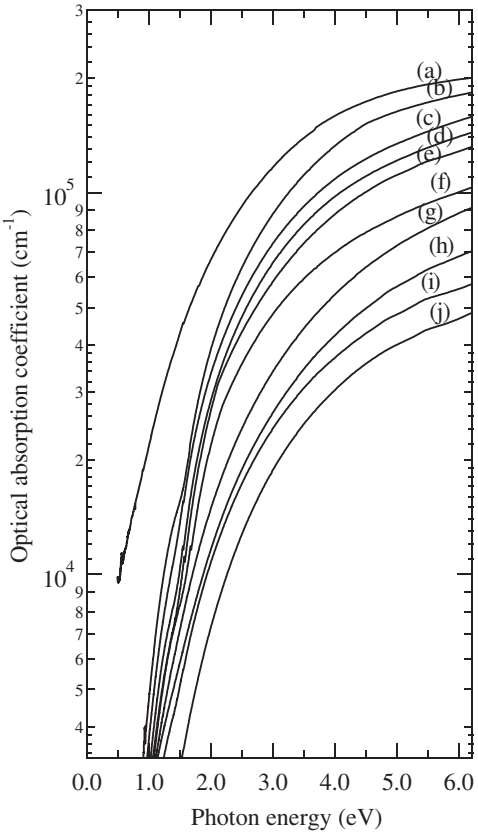

Figure 14. Optical absorption edge for different nitrogen partial pressures as a function of photon energy, deposited under various ambient nitrogen partial pressures.

undoped (sample A) up to about 30 mTorr and subsequently decreases with increasing NP up to 800 mTorr. The shape of the optical absorption edge in our experiment is similar to that of the absorption edge found for a-CN_x by Cheah *et al* [18] and amorphous Si by Cody *et al* [19]. Our result also agree with theirs [18, 19]: the absorption edge where it shifts towards the lower photon energy (higher wavelength) region with increasing NP has a reduction in transparency. This is evident, as we found that the reflectance is decreased while transmittance is observed to increase with increasing NP.

Our results are different to those of Bhattacharyya *et al* [20]: they have observed a gradual decrease of E_g with increase of N content. The decrease in σ_{RT} with N incorporation initially at 0.1 Torr may be due to the feature that as the N content increases from zero, the incorporated N atoms compensate the dangling bands in the a-C structure and increase the sp^3 fraction. For increasing of NP up to 1 mTorr and above 30 mTorr, the σ_{RT} is found to decrease, which may be due to an increasing density of sp^3 hybridization electronic states as shown by XPS, FTIR, and optical data relevant to band tails. At low NP up to 1 mTorr and upon increasing of NP above 30 mTorr, the variation of E_g and the electrical properties can be related to interstitial doping of N in C films through modifications of C–N bonding configurations by rearranging N in atoms.

However from 1 to 30 mTorr, the variation of E_g and the electrical properties can be related to graphitization of n-C:N films. Perhaps the doping of N accompanied by an increase

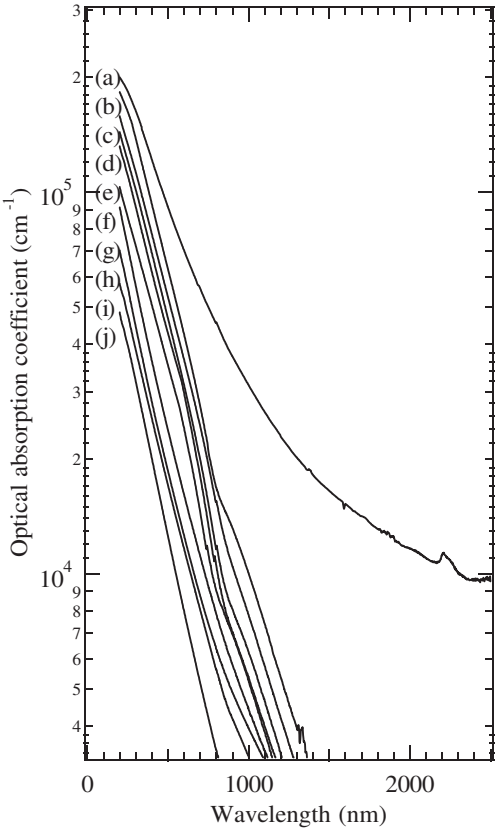

Figure 15. Optical absorption edge for different nitrogen partial pressures as a function of wavelength, deposited under various ambient nitrogen partial pressures.

of NP up to 30 mTorr increases the crystallinity and substitutional doping of N, thereby sharply increasing σ_{RT}. The increase of E_g (figure 13) and decrease of σ_{RT} (figures 12 and 13) with increasing N content (figure 4) above 30 mTorr can be related to the structural modification with increasing density of sp^2 hybridization electronic states as shown by XPS, FTIR, and optical data relevant to band tails. The surface morphological study of SEM and AFM has also shown the same phenomenon. Usually this kind of behaviour is observed for high contents of N in the carbon film, such as for the CN alloy [21, 22]. This n-C:N films might be promising for optical applications, as photoconductivity is reported by Nitta *et al* for CN alloyed film [23].

Photovoltaic solar cells of the configuration n-C:N/p-Si have been fabricated. A schematic diagram of the structure of the n-C:N films on p-type Si(100) substrates (n-C:N/p-Si) is shown in figure 16. From the I–V measurement, the I–V characteristics of the n-C:N/p-Si configuration photovoltaic solar cells, without light irradiation, displayed a rectifying I–V characteristic, indicating the formation of a heterojunction between the n-C:N films and Si substrates. The cell performances have been given by the dark I–V rectifying curve (figure 17) and I–V working curve (figure 18) under illumination when exposed to AM 1.5 illumination conditions (100 mW cm^{-2}, 25 °C). The figures show that the photovoltaic characteristics in the dark and under illumination are improved with increase of NP pressure up to 30 mTorr and deteriorate subsequently. As shown in figure 19, the open circuit voltage (V_{oc}) and short circuit current density (J_{sc}) for a cell deposited at 20 mTorr are found to be 273 mV and 8.12 mA cm^{-2},

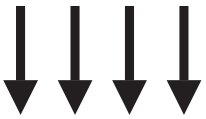

Gold (Au) electrode (Thickness: 15 nm) (Top contact)	
n-C:N film	(Thickness: 150-200 nm)
p-type Si	(Thickness: 350 μm)
Gold (Au) electrode (Thickness: 100 nm) (Back contact)	

Figure 16. Schematic diagram of the n-C:N/p-Si cell.

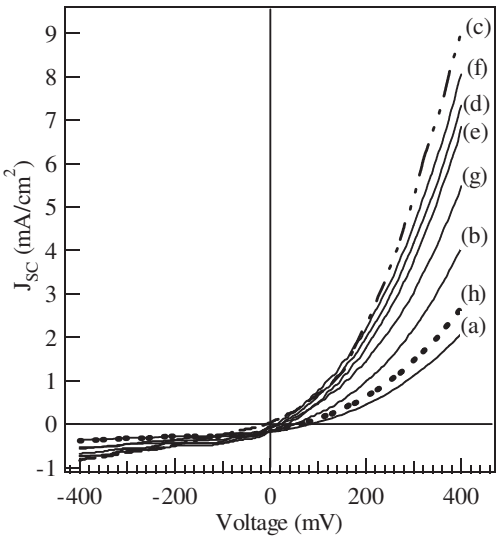

Figure 17. Current–voltage characteristics of the n-C:N/p-Si cell for dark deposition under various ambient nitrogen partial pressures: (a) 0.3, (b) 1, (c) 10, 20, 30, 50, 80, and 100 mTorr.

respectively. As can be seen from figure 20, the cell deposited at 20 mTorr shows efficiency (η) of (1.35%) and a fill factor of (FF) (49%). The maximum of V_{oc} and J_{sc} for the cells are observed for the cell deposited at 30 mTorr: approximately 292 mV and 9.02 mA cm^{-2}, respectively (figure 19). This cell shows that the highest energy conversion efficiency (η) and fill factor (FF) were found to be approximately 1.47% and 56%, respectively (figure 20).

4. Conclusions

Nitrogen doped n-type amorphous carbon (n-C:N) films are deposited by the pulsed laser deposition (PLD) technique at room temperature using a camphoric carbon target with different nitrogen partial pressures in the range from 0.1 to 800 mTorr. The influence of N-doping modification on the a-C films has been investigated. At low NP up to 1 mTorr and upon increasing of NP above 30 mTorr, the variation of the optical band gap (E_g) and electrical

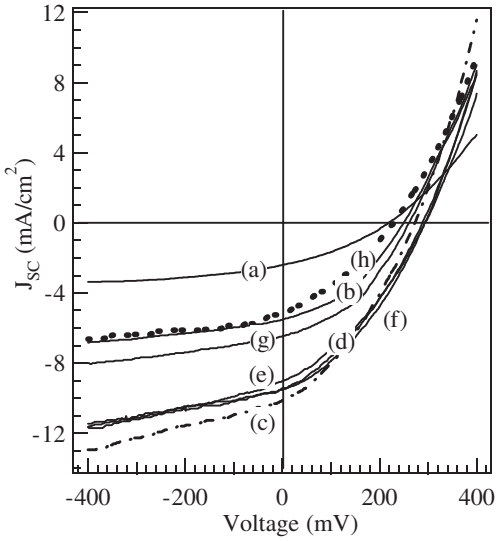

Figure 18. Current–voltage characteristics of the n-C:N/p-Si cell for illuminated deposition under various ambient nitrogen partial pressures: (a) 0.3, (b) 1, (c) 10, 20, 30, 50, 80, and 100 mTorr.

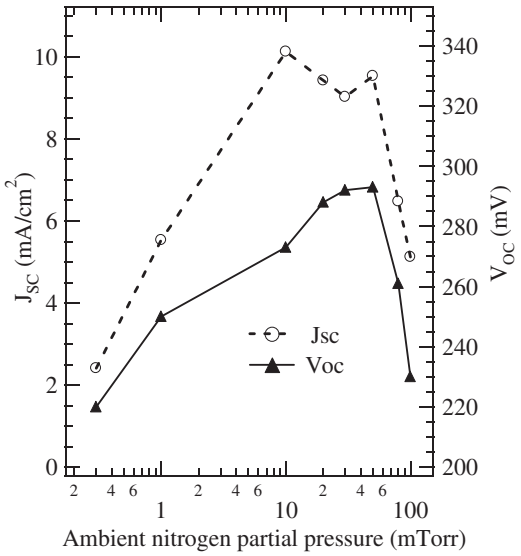

Figure 19. Short circuit current density plotted on the left axis and open circuit plotted on the right axis as a function of nitrogen partial pressures of the n-C:N/p-Si photovoltaic cell.

properties can be related to interstitial doping of N in C films through modifications of C–N bonding configurations by rearranging N in atoms. However from 1 to 30 mTorr, the variation of E_g and the electrical properties can be related due to graphitization of n-C:N films. The room temperature conductivity (σ_{RT}) is found to increase with N incorporation, perhaps due to increasing density of trihedral (sp^2) hybridization electronic states, as shown by x-ray photoelectron spectroscopy (XPS), Fourier transform infrared spectroscopy (FTIR), and optical data relevant to band tails. Study of the activation energy reveals that the Fermi level of

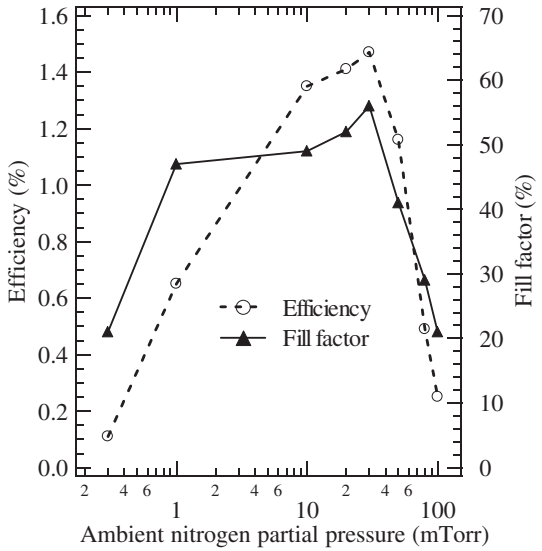

Figure 20. Efficiency plotted on the left axis and fill factor plotted on the right axis as a function of nitrogen partial pressures of the n-C:N/p-Si photovoltaic cell.

the n-C film moves from the valence band to near the conduction band edge through the mid-gap. The current–voltage photovoltaic characteristics of n-C:N/p-Si cells under 1 sun air-mass 1.5 (AM 1.5) illumination conditions (100 mW cm^{-2}, 25 °C) are improved up to 30 mTorr and deteriorate subsequently. The maximum open circuit voltage (V_{oc}) and short circuit current density (J_{sc}) for the cells are observed to be approximately 292 mV and 9.02 mA cm^{-2}, respectively. The highest energy conversion efficiency (η) and fill factor (FF) were found to be approximately 1.47% and 56%, respectively.

Acknowledgments

This work was supported by the Incorporated Administrative Agency New Energy and Industrial Technology Development Organization (NEDO) under the Ministry of Economy, Trade and Industry (METI) and 21st century COE programme at Nagoya Institute of Technology (NIT).

References

[1] Veerasamy V S, Amaratunga G A J, Davis C A, Timbs A E, Milne W I and Mackenzie D R 1993 *J. Phys.: Condens. Matter* **5** 169
[2] Kadas K, Ferenczy G G and Kugler S 1998 *J. Non-Cryst. Solids* **227** 367
[3] Zhou Z B, Cui R Q, Pang Q J, Hadi G M, Ding Z M and Li W Y 2002 *Sol. Energy Mater. Sol. Cells* **70** 487
[4] Cheah L K, Shi X, Liu E and Shi J R 1998 *Appl. Phys. Lett.* **73** 4273
[5] Veerasamy V S, Yuan J, Amaratunga G A J, Milne W I, Gilkes K W R, Weiler M and Brown L M 1993 *Phys. Rev.* B **48** 17954
[6] Jones D I and Stewart A D 1982 *Phil. Mag.* B **46** 423
[7] Alaluf M, Klibanov L and Croitoru N 1996 *Diamond Relat. Mater.* **5** 1497
[8] Veerasamy V S, Yuan J, Amaratunga G A J, Milne W I, Gilkes K W R, Weiler M and Brown L M 1993 *Phys. Rev.* B **48** 17954
[9] Rusop M, Mominuzzaman S M, Tian X M, Soga T, Jimbo T and Umeno M 2002 *Appl. Surf. Sci.* **197** 542

[10] Hammer P, Baker M A, Lenardi C and Gissler W 1997 *J. Vac. Sci. Technol.* A **15** 107
[11] Wixom M R 1990 *J. Am. Ceram. Soc.* **73** 1973
[12] Orzeszko S, Bala W, Fabisiak K and Rozploch F 1984 *Phys. Status Solidi* **81** 579
[13] Ronning C, Feldermann H, Merk P, Hofsass H, Reinke P and Thiele J U 1998 *Phys. Rev.* B **58** 2207
[14] Le Normand F, Hommet J, Szorenyi T, Fuchs C and Fogarassy E 2001 *Phys. Rev.* B **64** 235416
[15] Kusunoki I, Sakai M, Igari Y, Ishizuka S, Takami T, Takaoka T, Nishitani M and Ando T 2001 *Surf. Sci.* **492** 315
[16] Tauc J, Grigorovici R and Vancu A 1966 *Phys. Status Solidi* **15** 527
[17] Shi X, Cheah L K and Tay B K 1998 *Thin Solid Films* **312** 166
[18] Cheah L K, Shi X, Shi J R, Liu E J and Silva S R P 1998 *J. Non-Cryst. Solids* **242** 40
[19] Cody G D 1984 *Semiconductors and Semimetals* vol 21, Part B, ed J I Pankove (Orlando, FL: Academic) p 11
[20] Bhattacharyya S, Vallee C, Cardinaud C, Chauvet O and Turban G 1999 *J. Appl. Phys.* **85** 2162
[21] Anguita J V and Silva S R P 2000 *Diamond Relat. Mater.* **9** 777
[22] Chen D, Wei A, Wong S P and Peng S 1999 *Diamond Relat. Mater.* **8** 1130
[23] Nitta S, Takada N, Sugiyama K, Itoh T and Nonomura S 1998 *J. Non-Cryst. Solids* **230** 655